Membrane Thinning Effect of the β-Sheet Antimicrobial Protegrin†

William T. Heller,‡ Alan J. Waring,§ Robert I. Lehrer,|| Thad A. Harroun,‡ Thomas M. Weiss,‡ Lin Yang,‡ and Huey W. Huang*,‡

Department of Physics, Rice University, Houston, Texas 77251, Department of Pediatrics, Drew University-King Medical Center and University of California at Los Angeles, Los Angeles, California 90059, and Department of Medicine, University of California at Los Angeles School of Medicine, Los Angeles, California 90095

Received August 13, 1999; Revised Manuscript Received October 18, 1999

ABSTRACT: Lipid bilayers containing the antimicrobial peptide protegrin-1 (PG-1) were studied by lamellar X-ray diffraction. Previously, we have shown that the peptide exists in two distinct states when associated with lipid bilayers depending on the peptide concentration [Heller, W. T., Waring, A. J., Lehrer, R. I., and Huang, H. W. (1998) *Biochemistry 37*, 17331−17338]. For concentrations below a lipid-dependent threshold, PG-1 exhibits a unique oriented circular dichroism spectrum called the S state. X-ray experiments show that in this state PG-1 decreases the thickness of the lipid bilayer in proportion to the peptide concentration, similar to alamethicin's membrane thinning effect. This indicates that the S state is adsorbed in the headgroup region of the lipid bilayer, where the peptide is in an inactive state. For PG-1 above the threshold concentration, X-ray diffraction shows that the interaction between the peptide and the bilayer changes significantly. These results suggest that PG-1 has the same concentration-gated mechanism of action as alamethicin.

Protegrin-1 (PG-1),[1] an 18-amino acid peptide present in porcine leukocytes (*1*), is part of the pig's innate immune system. In vitro, the peptide can kill many bacteria, including *Escherichia coli* (*1*), *Listeria monocytogenes* (*1*, *2*), and *Neisseria gonorrhoeae* (*3*, *4*). It is also active against the fungus *Candida albicans* (*1*, *5*) and can protect cells from infection by HIV (*6*). The sequence of PG-1 is NH_2-RGGRLCYCRRRFCVCVGR-$CONH_2$.

PG-1 belongs to a family of innate host defense molecules called antimicrobial peptides, which were first discovered in the early 1980s. Other well-known antimicrobial peptides include cecropins, found in various insects (*7*) and perhaps also in tunicates (*8*) and pigs (*9*); the various types of defensins, found in mammals (*10*, *11*), insects (*12*), and plants (*13*); and magainin from the skin of the frog *Xenopus laevis* (*14*). Each of these host defense antimicrobials exhibits a somewhat unique spectrum of effectiveness against various microorganisms (*15*, *16*), and most apparently do not harm host cells significantly at peptide concentrations that destroy microorganisms. Experimental results have shown that antimicrobial peptides kill microbes by first binding to the surface and then inserting into the core of the microbial lipid membrane, thereby altering membrane permeability and impairing internal homeostasis (*15*). However, their precise molecular mechanisms are still not clear.

Many organisms also produce antibiotic peptides that are cytolytic to mammalian cells. Examples are alamethicin from the fungus *Trichoderma viride* (*17*) and melittin from the honeybee, *Apis mellifera* (*18*). Most host-defense and cytolytic peptides contain between approximately 20 and 40 amino acid residues. Their functional configurations vary, but most can be roughly divided into α-helices, β-sheets, or mixed structures. Mammalian defensins (*19*, *20*) and PG-1 (*21*, *22*) are folded into β-sheets linked by disulfide bonds. Insect defensins have an α-helix stabilized through disulfide bonds to twisted antiparallel β-sheets (*16*). Most other antimicrobials, including magainins, cecropins, alamethicin, and melittin, contain no cysteines, and are linear peptides that form α-helices when they bind membranes. At the moment, the significance of these structural differences is not entirely clear. The dimensions of most antimicrobial peptides are commensurate with the thickness of cell membranes, suggesting that they are capable of spanning the membrane as monomers. Even within the same helical category, there is no apparent characteristic difference, beyond that of amino acid sequence, between the cytotoxic melittin on one hand and the antimicrobial cecropins and magainins on the other. A better understanding of the molecular mechanisms that underlie peptide-mediated antimicrobial effects should enhance our ability to design and use such peptides for therapeutic and industrial applications.

To investigate the molecular mechanisms of antimicrobial peptides, lipid bilayers were used as model membranes. Most biochemical and biophysical studies have so far concentrated on the helical types, notably on alamethicin, melittin, and magainin, because of the relative simplicity of the helical

† H.W.H. was supported by NIH Grant GM55203 and NIH Training Grant GM08280, and by the Robert A. Welch Foundation; R.I.L. was supported by NIH Grants AI37945 and AI22839.

* To whom correspondence should be addressed: Department of Physics, Rice University, Houston, TX 77251-1892. Telephone: (713) 527-4899. Fax: (713) 527-9033. E-mail: huang@ion.rice.edu.

‡ Rice University.

§ Drew University-King Medical Center and University of California at Los Angeles.

|| University of California at Los Angeles School of Medicine.

[1] Abbreviations: PG-1, protegrin-1; DPhPC, 1,2-diphytanoyl-*sn*-glycero-3-phosphocholine; TFE, 2,2,2-trifluoroethanol; OCD, oriented circular dichroism; RH, relative humidity; *P*/*L*, peptide to lipid molar ratio.

10.1021/bi991892m CCC: $19.00 © 2000 American Chemical Society
Published on Web 12/08/1999

structure. One of the most significant results of all these experiments is the finding that these peptides exhibit two distinct states in lipid bilayers (*23*, *24*). For the helical peptides, one state is adsorbing in the lipid headgroup region with the helical axis oriented parallel to the plane of the bilayer and the other state exists as a transbilayer insertion into the hydrocarbon region with the helical axis oriented perpendicular to the plane of the bilayer. These two states are most easily distinguished by the method of oriented circular dichroism (OCD), which produces markedly different spectra for the two orientations of helices (*25*). Recently, we were surprised to find that the β-sheet PG-1 also exhibited two distinct states in lipid bilayers, each exhibiting a unique OCD spectrum (*26*), although the structural interpretations of these spectra are still lacking. However, the significance of the finding that all the peptides investigated so far exhibited two distinct states in lipid bilayers has not been widely appreciated.

Alamethicin has been studied for the longest, since the 1970s. For many years, it had been observed in either of the two states mentioned above by numerous investigators (see the references in ref *23*). Since it was thought that a peptide could only bind to lipid bilayers in one unique way, there was dispute as to which of the two states was correct (see ref *23* for the details). The issue was clarified by an experiment of OCD in which alamethicin was observed to make a reversible transition from one state to another via the change of the hydration level of the sample (*25*). The same transition was observed with the change of peptide concentration (*23*). Alamethicin tends to adsorb in the headgroup region (the surface state) at low concentrations. Above a certain threshold concentration, expressed in the peptide-to-lipid molar ratio *P*/*L*, a fraction of the peptide inserts into the membrane. The fraction increases rapidly with increasing *P*/*L* until all of the alamethicin has inserted across the bilayer. Since pores in the membranes were observed by neutron diffraction experiment only in the presence of the insertion state of alamethicin (*27*, *28*), the peptide insertion is likely the molecular mechanism of cytolysis. The existence of a concentration threshold, denoted as (*P*/*L*)*, for insertion can be regarded as a concentration gating for cytolysis. This (*P*/*L*)* varies greatly with the lipid composition of the bilayer (*23*, *29*). The lipid composition of the cell membrane determines not only the affinity for binding peptides from solution (e.g., the electrostatic effect) but also the threshold concentration for the peptide insertion (*23*, *29*). Thus, the cell type sensitivity to alamethicin can be at least partially explained by each cell's specific lipid composition in its membrane.

The concentration-gated mechanism is not unique to alamethicin. Subsequent studies showed that magainin appears to function by the same mechanism (*24*), although magainin formed a type of pores in membranes different from those of alamethicin (*30*). Preliminary investigation with melittin showed that it exhibits a similar transition from a surface state to an insertion state, and that this transition can be correlated with the formation of pores (*31*). Interestingly enough, the transition observed for PG-1 by OCD, while not able to be interpreted as a transition between two orientations of the peptide, suggests that PG-1 also has a concentration-gated mechanism of action (*26*).

PG-1 is folded into a β-hairpin stabilized by two disulfide bonds, according to solution NMR analyses (*21*, *22*). Its overall shape is roughly cylindrical, not very different from the shape of a helical peptide. Even so, the discovery of two distinct OCD states for PG-1 was not expected (*26*). Unlike helical peptides, for which the effect of orientation on their CD spectra is well understood (*25*), there is no corresponding theory for β-sheet peptides. It is not clear if the two distinct OCD spectra correspond to two different orientations of PG-1 or two distinct conformations of the molecule. Even more surprising than the discovery of two PG-1 states is the fact that there is a 1/1 correspondence between the states of PG-1 and the states of alamethicin (*26*). The reversible transition, which is a function of the level of hydration and *P*/*L*, between the two PG-1 states closely resembles the reversible insertion transition of alamethicin. Thus, we called the state of PG-1 that corresponds to the surface state of alamethicin the S state, and the state of PG-1 corresponding to the insertion state of alamethicin the I state. Similar to the case of alamethicin, the threshold concentration (*P*/*L*)* for the transition from the S state to the I state varies with the lipid composition of the membrane. Alamethicin is perhaps the most extensively studied membrane-active peptide. It is therefore useful to compare PG-1 to alamethicin by finding their similarities as well as their differences. In this paper, we report on our X-ray diffraction measurement performed on the S state of PG-1. We chose the lipid diphytanoylphosphatidylcholine (DPhPC) that provides the most experimentally convenient range of transition between the S state and the I state with a (*P*/*L*)* of 1/60. The results are compared with those from the same experiment performed on the surface state of alamethicin (*32*). We conclude that PG-1 in the S state is embedded in the headgroup region of the lipid bilayer that gives rise to a membrane thinning effect. This helps to explain the transition from the S state to the I state at high peptide concentrations.

MATERIALS AND METHODS

1,2-Diphytanoylphosphatidylcholine (DPhPC) was purchased from Avanti Polar Lipids (Alabaster, AL). The lipid was supplied in chloroform solution. Chloroform (HPLC grade) was purchased from Fisher Scientific (Pittsburgh, PA). 2,2,2-Trifluoroethanol (TFE) was purchased from Sigma (St. Louis, MO). All of the above materials were used without further purification. PG-1 was synthesized by SynPep Corp. (Dublin, CA) using Fmoc chemistry. The peptide was purified and folded according to the methods described by Harwig et al. (*2*). A stock solution of PG-1 in TFE was made for use in the sample preparation process.

Sample preparation for the X-ray diffraction measurements was similar to the procedure used in previous experiments (*26*). Glass substrates (1 cm^2) were cut from standard microscope slides (Fisher Scientific). The slide was abrasively cleaned using a tissue and ethanol. Then, the slide was placed in a bath of hot sulfuric and chromic acid for roughly 20 min. The slide was removed from the bath and rinsed with distilled water until there was no trace of acid. Next, the slide was rinsed with ethanol and placed in an oven ($\sim$70 °C) to dry. Once the slide had been dried, appropriate amounts of the stock lipid and peptide solutions were deposited on the slide in the desired peptide-to-lipid ratio (*P*/*L*). All samples were made with 0.5 mg of lipid and the

corresponding amount of peptide. The original solvent from the stock solutions was allowed to evaporate. Then, the sample was redissolved using a 6/1 chloroform/TFE solution and allowed to dry again. While the solvent dried, the sample self-assembled into an aligned multilamellar stack on the surface of the substrate. Good samples were clear with a smooth texture. The dried sample was placed in a vacuum freeze-drier for 1 h. Once removed from the freeze-drier, the sample was ready to be placed in the sample chamber for measurement.

The sample chamber controls the environment of the sample. The temperature of the sample and the relative humidity within the chamber were controlled. The sample chamber itself consists of a copper mount which affixes to a goniometer head and two plastic boxes, one inside the other so the inside box is insulated from room temperature. The copper mount is where the sample is placed, being affixed with heat-sink compound. The lids of the two boxes are also connected to the copper mount. Both boxes have entry and exit windows for the X-rays that are covered by Mylar and sealed with vacuum grease (Varian, Lexington, MA). The outer box is wrapped with electrical tape to reduce the amount of external light hitting the sample. The environmental controls are feedback circuits which respond to the outputs of temperature and relative humidity probes. The settings can be made either manually or by a computer. The feedback circuits provide heating and cooling using thermoelectric modules (Melcor Electronics Corp., Trenton, NJ). The temperature controller maintains the temperature of the copper mount, while the device for the relative humidity heats and cools a small water bath that is affixed to the chamber directly below the sample. The temperature probe is model AD590K (Omega Engineering, Inc., Stamford, CT), which is a surface-mount, solid-state device that has an absolute accuracy of ±1 °C. The temperature of the sample can be controlled to within ±0.3 °C. The relative humidity probe is model EMD-2000 (PhysChem Scientific, New York, NY), which utilizes a resistive polymer as the sensing element. It has an absolute accuracy of ±2% RH and makes it possible to control the RH to within ±0.3% RH. Both probes are affixed to the copper mount with heat-sink compound at the same height as the sample.

The X-ray diffraction experiments were performed using an Enraf-Nonious Diffractis 581 X-ray generator (Delft, The Netherlands) fitted with a normal focus copper anode sealed tube (K_α, $\lambda = 1.54$ Å) and a four-circle Huber goniometer (Rimsting, Germany). The window of the tube had a Ni filter to reduce the level of unwanted K_β X-rays. Additionally, an aluminum attenuator was employed at low angles to limit the diffracted intensity to less than 10 000 counts/s to maintain good counting statistics. The beam geometry was defined with two vertical slits, which provided a horizontal divergence of 0.23°, and a horizontal Soller slit, which provided a vertical divergence of 0.4°. Photons were counted using a proportional counter consisting of an adjustable, vertical slit, a graphite monochromator set to pass CuK_α X-rays, a NaI crystal, and a photomultiplier. A personal computer controlled the goniometer, the sample conditions, and the data collection. $\theta - 2\theta$ scans were run from 0.5° to 10° in θ with a 0.02° step size between data points. Data were collected and analyzed for P/Ls of 0, 1/140, 1/90, 1/70, and 1/30. Several samples were measured for each concentration. The two best quality samples, in terms of uniformity, number of diffraction orders observed, and quality of the sample mosaic, were kept for further analysis. Each sample was measured at 11−15 RH settings ranging from ∼70 to ∼100% RH. The temperature was maintained at 29.0 ± 0.3 °C. Four sets were collected per RH setting. The last three sets for a given RH setting did not change, and were considered to be in equilibrium.

Much of the data analysis followed that outlined in Wu et al. (*32*), but there were enough differences that the process must be briefly described. First, the equilibrated data sets for a given RH setting were averaged. Then, the instrumental background was removed. The background was significant for the higher orders of diffraction where the diffracted intensities become comparable to the background. To determine the background, all peaks found in the averaged data were replaced using a linear interpolation between points to the left and right of the maximum, which were well outside the width of the peak. This process was performed twice for each data set to ensure a background free from diffraction peaks. Then, all backgrounds generated in this manner for each sample at all the different RH settings were averaged to produce a clean, smooth background. The averaged background was subtracted from each averaged data set. The resulting data files contained only the diffraction peaks and noise.

The next step in the data reduction was to correct for the instrumental artifacts. The first correction made was for the dead time of the detector ($\tau = 4.4 \times 10^{-6}$ s). The arrival of photons at the detector was assumed to be a Poisson process. Therefore, the measured intensity is related to the actual intensity I_0 by $I_m = I_0 e^{-I_0 \tau}$. The equation is not invertible, so a spline interpolation was used to perform the correction. This was not a large correction, amounting to a few percent for an I_m of 10 000 s^{-1}. The next correction was for the attenuator used to limit the count rate for the lower orders of diffraction. The device attenuated the counts by a factor of 45.5; therefore, all data below the angle where the attenuator was turned off were multiplied by this factor. Then, the variation of the sample size relative to the beam size as a function of angle was corrected for. As the sample turns in the beam, it subtends a different solid angle to the X-ray source that varies with θ. This was a very important correction, particularly for small angles. The data were also corrected for polarization and for the Lorentz factor (*33*). Next, the data were corrected for the variation of the atomic form factor with the scattering angle using data from the International Tables for Crystallography (*34*). Finally, the data were corrected for absorption by the sample and the variation of diffraction volume with the angle of incidence in the manner described by Warren (*33*). The absorption coefficient was calculated for each sample on the basis of the sample composition and data from the International Tables for Crystallography (*34*).

The corrected diffraction peaks were fit with a Gaussian function to determine the angular position and the integrated intensity. The angular positions were translated into q, the momentum transfer of the X-ray scattering, which is related to the angle θ and the wavelength λ by $q = (4\pi/\lambda) \sin \theta$. The lamellar phase of a lipid bilayer has a single repeat spacing D. To determine the repeat spacing, a plot of q versus the diffraction index was fit with a straight line. The slope

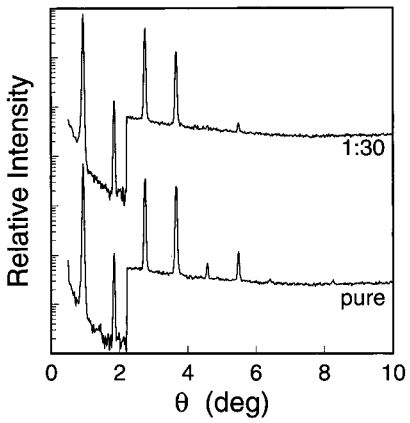

FIGURE 1: Representative diffraction patterns, one of pure DPhPC and one of PG-1 in DPhPC at a *P*/*L* of 1/30, the highest peptide concentration measured. Both are at a repeat spacing *D* of ~49.5 Å. The patterns are displaced vertically for clarity. All other samples produced patterns intermediate between these two.

of the curve q_1 is related to the repeat spacing *D* by $D = 2\pi/q_1$. The intercept of the curve, which was always very small, resulted from slight errors in the positioning of the sample in the beam. The diffraction amplitudes, without the phase information, are the square roots of the integrated intensity.

Generally, diffraction amplitudes are complex numbers of the form $Fe^{i\varphi}$, where *F* is the magnitude and φ is the phase. This phase information is lost because the measured intensity of a diffraction order $I = |Fe^{i\varphi}|^2$. Therefore, the next step in the data analysis was to determine the phases of the diffracted amplitudes. The symmetry of the system was such that the phases were either 0 or π. The use of different RH values during the experiment made it possible to use the swelling method (*35*) for phase determination. The electron density profile was constructed using the experimental data to perform a cosine transform

$$\rho(z) = \sum_{k=1}^{n} F_k e^{i\varphi_k} \cos(q_k z) \qquad (1)$$

where *n* is the total number of diffraction orders, $F_k e^{i\varphi_k}$ is the *k*th amplitude, and q_k is the momentum transfer of the *k*th diffraction order. The result is a relative electron density profile which is related to the actual number density of electrons ρ_o by $\rho = a\rho_o + b$ with constants *a* and *b*. Normalization is not necessary for determining the thickness of the bilayer from the profile. The thickness of the bilayer was measured by the separation between the two maxima in the electron density profile. This represents the distance from the phosphate group on one side of the bilayer to the phosphate group on the other.

RESULTS

Figure 1 shows two representative diffraction patterns collected: one of pure DPhPC without peptides and the other with PG-1 at a *P*/*L* of 1/30, the highest concentration that was measured. All the patterns we collected have a single series of diffraction peaks with one repeat spacing, demonstrating that the samples are in the lamellar phase. The diffraction patterns vary slightly and slowly with increasing *P*/*L*. The peptide is not forcing the lipid to adopt another structural phase, but is instead being incorporated into the lipid bilayers, producing slight changes in the structures of the bilayers. One obvious change as a function of *P*/*L* is the decreasing number of discernible diffraction peaks. This effect could be due to deteriorating sample quality caused by the presence of peptide. Multilayer samples with excessive defects produce damped diffraction patterns with decreased intensities and a smaller number of peaks, compared to a sample with few defects. Damped diffraction patterns give inaccurate results (*32*). Therefore, it is important that when a comparative study is made of a number of membrane samples, all samples should have equally good quality. To check whether this was the case, we examined the mosaic scan of each sample. This was done by a two-dimensional $\omega - 2\theta$ scan around a Bragg peak. The scan (Figure 2) gave the complete mosaic spread of the sample (*33*). We found that the mosaic spreads of all the samples were similar; therefore, the sample qualities of all *P*/*L*s were about the same. (We rejected samples exhibiting poorer qualities.) As a result, we are confident that the differences in the diffraction patterns are the result of changes in the structure of the bilayer, and not the result of differences in sample quality.

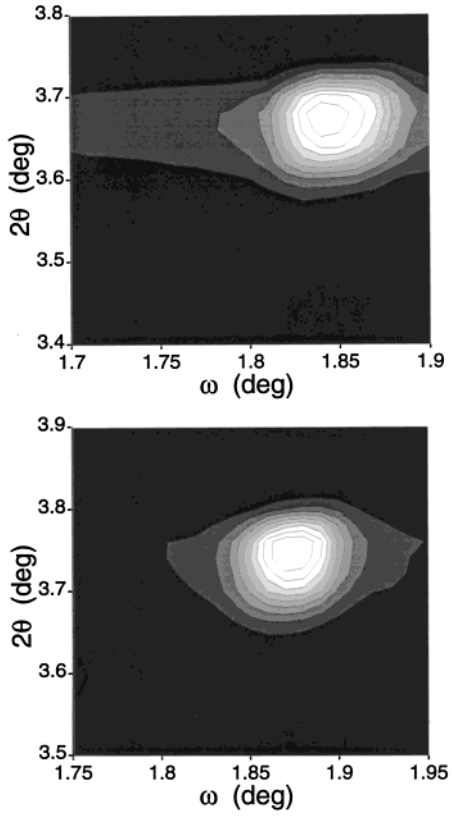

FIGURE 2: $\omega - 2\theta$ scan around the second Bragg peak for pure DPhPC (top) and PG-1/DPhPC at a *P*/*L* of 1/30 (bottom). Both exhibit a mosaic spread of ~0.05° (full width at half-maximum). All other samples exhibited comparable mosaic spreads. We rejected samples exhibiting poorer qualities.

Figure 3 shows the F_k values with the proper phasing. The signs of the amplitudes were chosen such that the data from different *D* spacings trace out a continuous curve. The smoothness of the series attests to the quality of the data and also to the fact that the bilayer structure of each sample changed little with changes in hydration. Figure 4 shows the electron density profiles of the lipid bilayers at various *P*/*L*s.

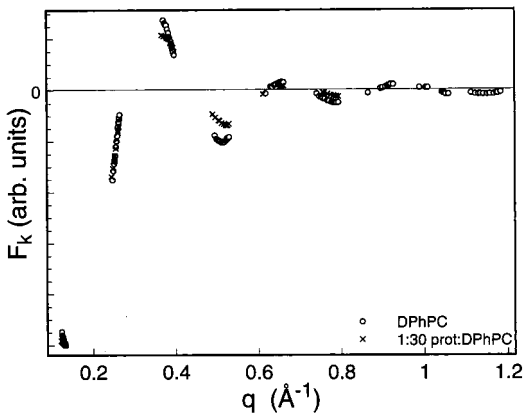

FIGURE 3: Phasing diagram for pure DPhPC and PG-1/DPhPC at a *P*/*L* of 1/30. The signs of the diffraction amplitudes were chosen so that the series of patterns at varying *D* spacings fall on a smooth curve.

The shapes of the electron density profiles show little change from $P/L = 0$, the pure lipid, through $P/L = 1/30$. The change of PG-1 from the state S to the state I, which occurs at $(P/L)^* = 1/60$ (*26*), does not significantly alter the shape of the bilayer. Only the central trough region becomes slightly more rounded as *P*/*L* increases. However, there is a definite trend of reducing the peak-to-peak distance as will be discussed below. Note that the electron densities of peptide, lipid, and water are such that at these *P*/*L*s the peptide is invisible in lamellar X-ray diffraction (*32*). What we detected were the profiles of the bilayer under the influence of the peptide.

It has been shown that the peak-to-peak distance (PtP) of the electron density profile is the most reliable quantity that can be measured by X-ray diffraction (*36*; W. C. Hung, F. Y. Chen, and H. W. Huang, unpublished results). The peak of the profile corresponds to the position of the phosphate in the lipid molecule. Thus, the PtP is a good measure of the membrane thickness. Figure 5 shows the PtPs of all the patterns we have measured as a function of *D* spacing. There clearly are two different groups of data present in the figure. The data for concentrations with a $(P/L)^*$ of less than ~1/60 form one group, and the data for a *P*/*L* of 1/30 stand out as an exception. The pure lipid and low-*P*/*L* bilayers have more or less parallel PtP curves. Most importantly, the PtP at a given *D* spacing decreases systematically with *P*/*L* for these concentrations. On the other hand, the PtP curve for a *P*/*L* of 1/30 has a slope different from all the others. It also breaks the trend of decreasing PtP with increasing *P*/*L*.

DISCUSSION

The results of these experiments are very interesting in light of the previous work done by this group on PG-1 in DPhPC (*26*). OCD experiments showed that PG-1 undergoes a transition in DPhPC as a function of *P*/*L* from an S state below a $(P/L)^*$ of ~1/60 to an I state above (*26*). It was noted that there is a great deal of similarity between the transition observed for PG-1 and alamethicin's insertion transition (*23*, *29*). This led to the suggestion that the two transitions are driven by the same mechanism. In this paper, measurements of the membrane thickness show that the DPhPC bilayer is thinned by the peptide for concentrations below $(P/L)^*$. Above $(P/L)^*$, the interaction between PG-1 and DPhPC changes in a way which suggests that the interaction between the bilayer and the peptide has changed significantly. Similar behavior was observed for alamethicin in DPhPC by X-ray diffraction (*32*, *37*), again suggesting that the transition observed by OCD is driven by the same mechanism.

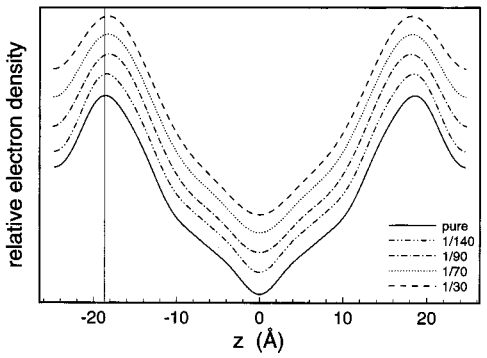

FIGURE 4: Unnormalized electron density profiles, all with a repeat spacing *D* of ~49.5 Å. The profiles are shifted vertically for clarity. The vertical line is the peak position of pure DPhPC. All other profiles have smaller PtPs.

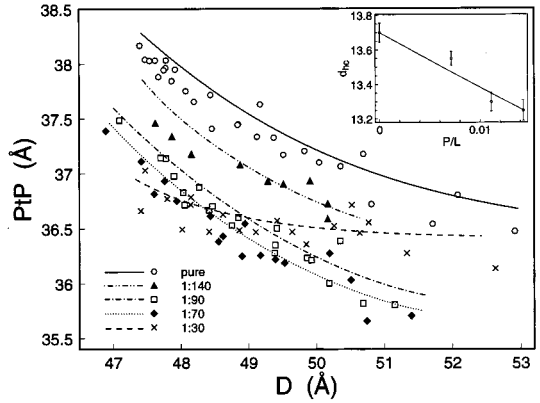

FIGURE 5: PtP of the bilayer plotted as a function of the repeat spacing *D*. The lines in the figure are intended as a guide for the eye. For a *P*/*L* of <1/60, the membrane thins in proportion to *P*/*L*. Above a *P*/*L* of 1/60, the membrane thins less at high *D* (close to full hydration). The inset shows the thickness of the hydrocarbon core of the bilayer d_{hc} as a function of *P*/*L*. The solid curve is the least-squares fit using eq 2. The error bars represent the root-mean-square deviation from the least-squares fit to the data shown in the main frame.

We believe that alamethicin's insertion transition (*23*, *29*) is driven by the membrane thinning effect (*29*, *32*, *37*). Alamethicin in low concentrations tends to adsorb into the headgroup region of the bilayer. This action expands the headgroup region laterally. Concurrently, the hydrocarbon chains undergo trans-gauche conformation changes to accommodate the lateral expansion (see the illustration in Figure 7 of ref *40*). (In this experiment, the peptides are symmetrically absorbed on both sides of the lipid bilayer.) The average thickness of the bilayer decreases because the chain volume is practically constant under the trans-gauche excitations (*38*). The energy cost of this lateral expansion is proportional to the square of the degree of thinning (*39*). Since the degree of thinning is approximately proportional to the concentration of alamethicin *P*/*L*, the free energy of surface adsorption by peptides contains a positive term that increases quadratically with *P*/*L*. Once the concentration of alamethicin reaches a critical value $(P/L)^*$, it becomes

energetically favorable for the peptide to insert across the bilayer rather than to be adsorbed on the surface. Thus, we regard the transition between the inactive, surface state and the membrane-spanning active state as being driven by the energy cost of the deformation of the bilayer produced by the peptides adsorbed in its headgroup region (*29*, *37*). We called this mechanism the membrane thinning effect (*40*).

The membrane thinning data presented here support the hypothesis that the transition of PG-1 observed by OCD is driven by the same mechanism. It is possible to calculate the areal expansion of the bilayer due to PG-1 and determine if it is consistent with the cross-sectional area of the peptide. As mentioned, the volume of the hydrocarbon chains is constant. Therefore, the thickness of the chains is inversely proportional to the area in the plane of the bilayer. When there is peptide in the headgroup region, the average area per lipid is the area of the unperturbed lipid plus the area of the peptide times P/L. Therefore, the thickness of the hydrocarbon chains, as a function of P/L, is given by (*40*)

$$d_{hc} = \frac{A_L d_{hc0}}{A_L + (P/L)A_P} \cong d_{hc0}\left[1 - \frac{A_P}{A_L}\left(\frac{P}{L}\right)\right] \qquad (2)$$

where d_{hc0} is the unperturbed thickness of the hydrocarbon chains, A_L is the area of the unperturbed lipid, and A_P is the area per peptide. As will be shown below, $A_P/A_L \sim 3$; thus, when $P/L < 1/60$, the linear approximation of eq 2 is valid. The thickness of the hydrocarbon chains is obtained by one-half of PtP minus the distance from the phosphate to the edge of the chain region. The latter has been estimated to be 4.85 Å (W. C. Hung, F. Y. Chen, and H. W. Huang, unpublished results; *41*). A d_{hc0} value of 13.7 Å is obtained from the PtP of pure DPhPC at high D. The area per lipid of DPhPC is ~82 Å^2, based on the thickness determined from the X-ray diffraction at a high level of hydration and the molecular volume of 1588 Å^3 (*32*).

d_{hc} is plotted as a function of P/L for concentrations below $(P/L)^*$ in the inset of Figure 5. The data are roughly linear. The solid line is the fit using eq 2. The fit gave the areal expansion per PG-1 molecule (195 ± 40 Å^2). This number can be compared to the values determined from the molecular structure of PG-1 (*21*, *22*). The area of PG-1 parallel to the long axis of the molecule is ~240 Å^2, while the area as viewed along the length of the molecule is ~100 Å^2. Thus, the value from the thinning data suggests that the peptide is adsorbing into the headgroup region of the bilayer with the long axis of the peptide parallel to the plane of the bilayer. These results indicate that the OCD spectrum S of PG-1 is produced when the long axis of the molecule is perpendicular to the incident light. There is a possible explanation for why A_P from the fit using eq 2 is lower than that from the NMR structure. PG-1 may displace some of the water molecules associated with the headgroup. If this occurs, the apparent areal expansion of the bilayer due to the peptide adsorption will be smaller than that predicted by the structure of the peptide and the amount of thinning would be reduced from the simple model described by eq 2.

This could explain the difference between the A_P determined for alamethicin in ref *32* and PG-1 here, even though their molecular structures (*21*, *22*, *42*) indicate that they are approximately the same size. The area per alamethicin was determined to be ~280 Å^2, which is higher than the value ~195 Å^2 found here for PG-1. We found that the lipid bilayer responded differently to the two peptides. In the case of alamethicin, the degree of thinning is a function of the level of hydration for concentrations both above and below $(P/L)^*$ (*32*, *37*). Therefore, the choice of D spacing affects the extent of thinning determined for alamethicin. The degree of thinning by PG-1 is rather independent of hydration for concentrations below $(P/L)^*$. The previous work on alamethicin only measured the thickness of the bilayer up to a D of ~49 Å (*32*), whereas the current work measured D to ~53 Å. Over the range of D from ~47 to ~53 Å, the PtP decreases approximately 1.5 Å. In ref *32*, the degree of thinning for alamethicin was read from low levels of hydration, where the possible effect of water displacement mentioned above might be significantly reduced, and the thinning effect might be more closely described by the simple model in eq 2. Thus, the effect of water displacement is a possible explanation for the smaller area per PG-1 determined here. This effect will be more extensively investigated in the future.

The X-ray diffraction results for concentrations above $(P/L)^*$ show that the membrane relaxes back toward the thickness of the unperturbed bilayer and that the hydration dependence of the PtP lessens. This indicates that PG-1 has adopted a conformation different from the surface state that changes the hydrophobic matching between the bilayer and peptide. One possible explanation is the formation of a membrane-spanning pore. In the event that the peptide penetrates the hydrocarbon core of the bilayer and forms a pore similar to that of alamethicin (*27*, *28*), then a difference in the hydrophobic thickness of the peptide and the bilayer could produce the observed change in the membrane thickness. If PG-1 produces toroidal pores similar to those observed for magainin (*30*), then the bilayer may also tend to thicken. In a toroidal pore, the leaflets of the bilayer fold over onto each other, producing a pore which looks like the inside of a torus lined with peptide molecules. There is a free energy cost associated with the bilayer folding over onto itself. The larger the radius of curvature, the lower the free energy cost. Therefore, the membrane would tend to thicken when toroidal pores are present. Both of these models for the I state (the high-concentration, high-hydration level state) of PG-1 could explain the way that the thickness of the bilayer responds to the presence of the peptide. Neutron scattering experiments with PG-1 are in preparation which should be able to detect the presence of a pore and determine its structure.

In conclusion, this work shows that PG-1 changes the structure of DPhPC bilayers. Below $(P/L)^*$, it produces a level of membrane thinning in proportion to its concentration. The area per peptide deduced from the data is consistent with the molecule being adsorbed into the headgroup region of the bilayer with the long axis of the peptide parallel to the plane of the membrane. From these results, it can be concluded that the OCD spectrum S represents the surface state of the PG-1 and that the transition of PG-1 observed by OCD is driven by membrane thinning, much like the insertion transition of alamethicin (*23*, *29*, *32*, *37*). The changes in membrane thickness above $(P/L)^*$ clearly indicate that the hydrophobic matching between PG-1 and the bilayer has changed.

REFERENCES

1. Kokryakov, V. N., Harwig, S. S. L., Panyutich, E. A., Shevchenko, A. A., Aleshina, G. M., Shamova, O. V., Korneva, H. A., and Lehrer, R. I. (1993) *FEBS Lett. 327*, 231−236.
2. Harwig, S. S. L., Waring, A., Yang, H. J., Cho, Y., Tan, L., and Lehrer, R. I. (1996) *Eur. J. Biochem. 240*, 352−357.
3. Qu, X.-D., Harwig, S. S. L., Oren, A., Shafer, W. M., and Lehrer, R. I. (1996) *Infect. Immun. 64*, 1240−1245.
4. Qu, X.-D., Harwig, S. S. L., Shafer, W. M., and Lehrer, R. I. (1997) *Infect. Immun. 65*, 636−639.
5. Cho, Y., Turner, J. S., Dinh, N.-N., and Lehrer, R. I. (1998) *Infect. Immun. 66*, 2486−2493.
6. Tamamura, H., Murakami, T., Horiuchi, S., Sugihara, K., Otaka, A., Takada, W., Ibuka, T., Waki, M., Yamamoto, N., and Fujii, N. (1995) *Chem. Pharm. Bull. 43*, 853−858.
7. Hultmark, D., Steiner, H., Rasmuson, T., and Bowman, H. G. (1980) *Eur. J. Biochem. 106*, 7−16.
8. Zhao, C., Liaw, L., Lee, I. H., and Lehrer, R. I. (1997) *FEBS Lett. 412*, 144−148.
9. Lee, J. Y., Boman, A., Chuanxin, S., Andersson, M., Jornvall, H., Mutt, V., and Boman, H. G. (1989) *Proc. Natl. Acad. Sci. U.S.A. 86*, 9159−9162.
10. Ganz, T., Selsted, M. E., Harwig, S. S. L., Daher, K., Bainton, D. F., and Lehrer, R. I. (1985) *J. Clin. Invest. 76*, 1427−1435.
11. Ganz, T., and Weiss, J. (1997) *Semin. Hematol. 34*, 343−354.
12. Lambert, J., Keppi, E., Dimarcq, J.-L., Wicker, C., Reichhart, J.-M., Dunbar, B., Lepage, P., van Dorsselaer, A., Hoffmann, J., Fothergill, J., and Hoffmann, D. (1989) *Proc. Natl. Acad. Sci. U.S.A. 86*, 262−266.
13. Garcia-Olmedo, F., Molina, A., Alamillo, J. M., and Rodriguez-Palenzuela, P. (1998) *Biopolymers 47*, 479−491.
14. Zasloff, M. (1987) *Proc. Natl. Acad. Sci. U.S.A. 84*, 5449−5453.
15. Martin, E., Ganz, T., and Lehrer, R. I. (1995) *J. Leukocyte Biol. 58*, 128−136.
16. Hoffmann, J. A., Katatos, F. C., Janeway, C. A., Jr., and Ezekowitz, R. A. B. (1999) *Science 284*, 1313−1318.
17. Pandey, R. C., Cook, J. C., and Rinehart, K. L. (1977) *J. Am. Chem. Soc. 99*, 8469−8483.
18. Habermann, E. (1972) *Science 177*, 314−322.
19. Pardi, A., Zhang, X. L., Selsted, M. E., Skalicky, J. J., and Yip, P. F. (1992) *Biochemistry 31*, 11357−11364.
20. Cornet, B., Bonmatin, J.-M., Hetru, C., Hoffmann, J. A., Ptak, M., and Vovelle, F. (1995) *Structure 3*, 435−448.
21. Aumelas, A., Mangoni, M., Roumestand, C., Chiche, L., Despaux, E., Grassy, G., Calas, B., and Chavanieu, A. (1996) *Eur. J. Biochem. 237*, 575−583.
22. Fahrner, R. L., Dieckmann, T., Harwig, S. S. L., Lehrer, R. I., Eisenberg, D., and Feigon, J. (1996) *Chem. Biol. 3*, 543−550.
23. Huang, H. W., and Wu, Y. (1991) *Biophys. J. 60*, 1079−1087.
24. Ludtke, S. J., He K., Wu, Y., and Huang, H. W. (1994) *Biochim. Biophys. Acta 1190*, 181−184.
25. Wu, Y., Huang, H. W., and Olah, G. A. (1990) *Biophys. J. 57*, 797−806.
26. Heller, W. T., Waring, A. J., Lehrer, R. I., and Heller, W. T. (1998) *Biochemistry 37*, 17331−17338.
27. He, K., Ludtke, S. J., Worcester, D. L., and Huang, H. W. (1995) *Biochemistry 34*, 15614−15618.
28. He, K., Ludtke, S. J., Worcester, D. L., and Huang, H. W. (1996) *Biophys. J. 70*, 2659−2666.
29. Heller, W. T., He, K., Ludtke, S. J., Harroun, T. A., and Huang, H. W. (1997) *Biophys. J. 73*, 239−244.
30. Ludtke, S. J., He, K., Heller, W. T., Harroun, T. A., Yang, L., and Huang, H. W. (1996) *Biochemistry 35*, 13723−13728.
31. Harroun, T. A. (1999) Ph.D. Thesis, Rice University, Houston, TX.
32. Wu, Y., He, K., Ludtke, S. J., and Huang, H. W. (1995) *Biophys. J. 68*, 2361−2369.
33. Warren, B. E. (1969) *X-ray Diffraction*, pp 27−40, Dover Publications, Inc., Mineola, NY.
34. MacGillavry, C. H., and Reick, G. D., Eds. (1968) *International Tables for X-ray Crystallography, Volume III: Physical and Chemical Tables*, The Kynoch Press, Birmingham, England.
35. Blaurock, A. E. (1971) *J. Mol. Biol. 56*, 35−52.
36. Chen, F. Y., Hung, W. C., and Huang, H. W. (1997) *Phys. Rev. Lett. 79*, 4026−4029.
37. He, K., Ludtke, S. J., Heller, W. T., and Huang, H. W. (1996) *Biophys. J. 71*, 2669−2679.
38. Nagle, J. F., and Wilkinson, D. A. (1978) *Biophys. J. 23*, 159−175.
39. Huang, H. W. (1995) *J. Phys. II 5*, 1427−1431.
40. Ludtke, S. J., He, K., and Huang, H. W. (1995) *Biochemistry 34*, 16764−16769.
41. Sun, W.-J., Suter, R. M., Knewtson, M. A., Worthington, C. R., Tristram-Nagle, S., Zhang, R., and Nagle, J. F. (1994) *Phys. Rev. E49*, 4665.
42. Fox, R. O., and Richards, F. M. (1982) *Nature 300*, 325−330.

BI991892M